Rare Metal Materials and Engineering
Volume 54, Issue 1, January 2025
Available online at www.rmme.ac.cn

Science Press

Cite this article as: Zhou Jianan, Luo Ning, Liang Hanliang, et al. Microstructure Analysis of TC4/Al 6063/Al 7075 Explosive Welded Composite Plate via Multi-scale Simulation and Experiment[J]. Rare Metal Materials and Engineering, 2025, 54(01): 27-38. DOI: 10.12442/j.issn.1002-185X.20240504.

ARTICLE

Microstructure Analysis of TC4/Al 6063/Al 7075 Explosive Welded Composite Plate via Multi-scale Simulation and Experiment

Zhou Jianan[1,2], Luo Ning[1,2], Liang Hanliang[2], Chen Jinhua[2], Liu Zhibing[2], Zhou Xiaohong[2]

[1] National Key Laboratory of Intelligent Construction and Healthy Operation and Maintenance of Deep Underground Engineering, China University of Mining and Technology, Xuzhou 221116, China; [2] China Coal Technology Engineering Group Huaibei Blasting Technology Research Institute Limited Company, Huaibei 235000, China

Abstract: Because of the challenge of compounding lightweight, high-strength Ti/Al alloys due to their considerable disparity in properties, Al 6063 as intermediate layer was proposed to fabricate TC4/Al 6063/Al 7075 three-layer composite plate by explosive welding. The microscopic properties of each bonding interface were elucidated through field emission scanning electron microscope and electron backscattered diffraction (EBSD). A methodology combining finite element method-smoothed particle hydrodynamics (FEM-SPH) and molecular dynamics (MD) was proposed for the analysis of the forming and evolution characteristics of explosive welding interfaces at multi-scale. The results demonstrate that the bonding interface morphologies of TC4/Al 6063 and Al 6063/Al 7075 exhibit a flat and wavy configuration, without discernible defects or cracks. The phenomenon of grain refinement is observed in the vicinity of the two bonding interfaces. Furthermore, the degree of plastic deformation of TC4 and Al 7075 is more pronounced than that of Al 6063 in the intermediate layer. The interface morphology characteristics obtained by FEM-SPH simulation exhibit a high degree of similarity to the experimental results. MD simulations reveal that the diffusion of interfacial elements predominantly occurs during the unloading phase, and the simulated thickness of interfacial diffusion aligns well with experimental outcomes. The introduction of intermediate layer in the explosive welding process can effectively produce high-quality titanium/aluminum alloy composite plates. Furthermore, this approach offers a multi-scale simulation strategy for the study of explosive welding bonding interfaces.

Key words: TC4/Al 6063/Al 7075 composite plate; explosive welding; microstructure analysis; multi-scale simulation

With the rapid development of modern industries such as aerospace, automotive, and chemical industries, the performance requirements for materials become increasingly stringent. Single metal materials often cannot meet the functional demands of specific environments. By combining two or more metals to form a layered composite structure, it is possible to improve material performance in a targeted manner by leveraging the properties of various metal materials based on actual needs[1–2]. For example, Ti/Al layered composites possess not only the advantages of aluminum alloys, such as low density, high electrical and thermal conductivity, and low cost, but also the high strength, high-temperature resistance, and good corrosion resistance of titanium alloys[3–4]. Consequently, these materials have been extensively utilized across a multitude of sectors.

The fabrication of Ti/Al dissimilar metal composite plates presents significant challenges due to substantial differences in thermal conductivity, melting points, and coefficients of thermal expansion between the two materials[5–6]. Additionally, they are highly reactive with oxygen and nitrogen in the air at high temperatures, making traditional welding techniques unsuitable for effectively joining these materials[7]. Explosive

Received date: August 11, 2024
Foundation item: Opening Foundation of Key Laboratory of Explosive Energy Utilization and Control, Anhui Province (BP20240104); Graduate Innovation Program of China University of Mining and Technology (2024WLJCRCZL049); Postgraduate Research & Practice Innovation Program of Jiangsu Province (KYCX24_2701)
Corresponding author: Luo Ning, Ph. D., Professor, National Key Laboratory of Intelligent Construction and Healthy Operation and Maintenance of Deep Underground Engineering, China University of Mining and Technology, Xuzhou 221116, P. R. China, Tel: 0086-516-83590666, E-mail: nluo@cumt.edu.cn

welding is a unique manufacturing technique for layered composite materials, which utilizes high-speed collisions induced by explosives to achieve a high-strength metallurgical bonding within microseconds. This technique has found widespread application in the production of dissimilar metal composites that cannot be fabricated by conventional welding processes, due to its superior welding quality[8–10].

Currently, extensive research has been conducted on the explosive welding of Ti/Al composite plates and the mechanical properties of the resulting samples[11]. With the continuous evolution of technology for fabricating Ti/Al composite materials, researchers are increasingly eager to enhance the mechanical performance of Ti/Al alloy laminated composite plates. Compared with the Ti/Al composite materials produced in previous studies, the TC4 titanium alloy and Al 7075 aluminum alloy exhibit superior mechanical properties and material characteristics. However, the high hardness and strength of the base materials narrow the explosive welding window, posing a challenge to achieve high-quality composites. To address these challenges, interlayer techniques have been introduced for the explosive welding fabrication process to resolve the welding issues between dissimilar materials with significantly different properties. Previous studies have confirmed the effectiveness of introducing interlayer materials[12].

Under the influence of the detonation wave from explosives, intense collision of welding materials, interatomic interactions and diffusion at the welding interface, as well as the overall morphological evolution of the interface are key factors affecting the quality of material bonding. Due to violent release of energy from the explosive detonation and rapid bonding process in explosive welding, current experimental testing techniques are unable to observe the formation and evolution of the interface and the interatomic interactions during the explosive welding process[13–14]. To further reveal the multi-scale evolution characteristics of the explosive welding interface, numerical simulation has been applied to the field of explosive welding. Advanced computational methods such as Eulerian, Arbitrary Lagrangian-Eulerian (ALE), and smoothed particle hydrodynamics (SPH) are instrumental in visualizing substantial plastic deformation occurring at material interfaces during high-speed impacts, which are all observable at the optico-microscopic scale. Complementarily, molecular dynamics (MD) simulations delve into the atomic-scale realm, offering insights into the intricate processes of atomic diffusion[15–17]. However, previous studies often focus on the formation characteristics of the interface at a single scale, and there is a lack of further research on how to effectively combine numerical simulations of explosive welding at different scales.

To address the aforementioned challenges, this study introduced an interlayer technique to fabricate TC4/Al 6063/Al 7075 composite plates using explosive welding. Microscopic structure at the joining interface was characterized and analyzed by field emission scanning electron microscope (FESEM) and electron backscattered diffractometer (EBSD), the interface morphology and grain characteristics were observed, and the elemental distribution across the interface was quantified. Furthermore, an innovative approach combining the finite element method (FEM)-SPH at optico-microscopic scale and MD at microscopic scale was proposed. This approach revealed the characteristics of interface morphology, temperature, and pressure distribution at the optico-microscopic scale. Using the initial collision parameters obtained from the aforementioned simulations, MD simulations were conducted to analyze the atomic-scale interfacial bonding and diffusion evolution mechanism, and to derive the thickness of the diffusion layer.

1 Explosive Welding Experiment

TC4 was selected as the flyer plate, with Al 6063 as the interlayer plate and Al 7075 as the substrate. The interlayer and substrate were placed parallelly to the flyer plate, positioned below it. The experimental setup for the explosive welding of the TC4/Al 6063/Al 7075 composite plate is depicted in Fig. 1. The dimension of the flyer plate was 150 mm×100 mm×2 mm, the interlayer plate dimension was 180 mm×120 mm×1 mm, and the substrate plate dimension was 150 mm×100 mm×2 mm. The plates were laid parallelly on a hardened sand surface, and aluminum spacers of varying heights were placed at the four corners between the plates. The gap between the TC4 and Al 6063 plates was set to 5 mm, while the gap between the Al 7075 and Al 6063 plates was set to 4 mm. Prior to the experiment, the welding surfaces were ground with sandpaper and cleaned with acetone to remove the surface oxide layer, ensuring a smooth and clean surface for welding. The experiment utilized emulsified powder explosives, and the detonation velocity was controlled at approximately 2100 m/s by incorporating quartz sand, with a density of about 0.8 g/cm³ and a thickness of 25 mm for the explosive layer. The explosives were initiated by an electronic detonator, which propelled the TC4 plate to collide the Al 6063 plate. Upon effective joining of the flyer and interlayer plates, the resulting composite plate collided with the substrate, achieving the final composite structure.

To further characterize the microstructure of the bonding interface, the samples were sectioned along the detonation direction by wire cutting. The samples were polished with sandpaper from low to high grit numbers, followed by mechanical polishing with metallographic grinder. After

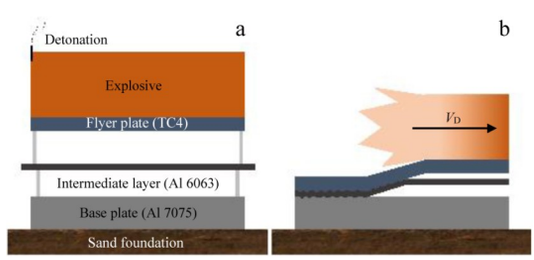

Fig.1 Schematic diagrams of parallel welding device (a) and explosive welding process (b) for TC4/Al 6063/Al 7075

mechanical polishing, argon ion polishing was employed to meet the characterization and testing requirements. Under an acceleration voltage of 10 kV, the micromorphology and elemental distribution of the joining interface were characterized by FESEM model MAIA3 LMH. Subsequently, at an acceleration electric potential of 20 kV with duration of 5 s in high-beam mode, the EBSD model Symmetry S2 was used to collect data of the grains near the bonding interface.

2 Simulation Method

2.1 FEM-SPH simulation procedure

In order to investigate the interfacial morphology, temperature, and pressure distribution characteristics in the explosive welding of TC4/Al 6063/Al 7075, a FEM-SPH numerical model was developed by the commercial software ANSYS/AUTODYN 2D. The FEM-SPH model effectively mitigates the computational issues related to mesh distortion that are inherent in purely FEM models while precisely capturing the wavefront interface features of the explosive welding process. Furthermore, it offers improved computational efficiency over a standalone SPH model and ensures the fidelity of the detonation simulation. The specific parameters for this simulation are shown in Table 1–3. The explosive material was characterized by the Jones-Wilkins-Lee (JWL) equation of state, which provides an accurate representation for the expansion and energy transfer during the detonation of the explosive products. Eq. (1) is essential for the precise simulation of the explosive welding process and gaining insights into the physical phenomena occurring at the bonding interface[18].

$$P = A\left(1 - \frac{\omega}{R_1 V}\right)e^{-R_1 V} + B\left(1 - \frac{\omega}{R_2 V}\right)e^{-R_2 V} + \frac{\omega e}{V} \tag{1}$$

where P is the pressure of the detonation product, V is the relative specific volume of the detonation product, and e is the initial specific internal energy; A, B, R_1, R_2, and w are JWL parameters.

The constitutive model for the experimental plates was established using the Steinberg-Guinan strength model, which offers enhanced accuracy in simulating the near-fluid behavior of metals at strain rates exceeding 10^{-5} s^{-1} [17]. The specific form is shown in Eq.(2–3):

$$G = G_0\left[1 + \frac{G'_P}{G_0}\cdot\frac{P}{\eta} + \frac{G'_T}{G_0}(T - 300)\right] \tag{2}$$

$$Y = Y_0\left[1 + \frac{Y'_P}{Y_0}\cdot\frac{P}{\eta^{1/3}} + \frac{G'_T}{G_0}(T - 300)\right](1 + \beta\varepsilon)^n \tag{3}$$

where β is the hardening constant parameter, n is the hardening index parameter, ε is the effective plastic strain, T is temperature, and η is the compression parameter.

The SHOCK state law was used to delineate the mathematical relationships between physical quantities such as density, pressure, and internal energy during the shock impact on the plates[19]. This model is pivotal for depicting the alterations in material properties under extreme conditions, such as elevated temperatures and pressures. The specific forms are shown in Eq.(4–7).

$$P = P_{\mathrm{H}} + \Gamma\rho(e - e_{\mathrm{H}}) \tag{4}$$

$$P_{\mathrm{H}} = \frac{\rho_0 C_0^2 \mu(1 + \mu)}{\left[1 - (S - 1)\mu\right]^2} \tag{5}$$

$$e_{\mathrm{H}} = \frac{1}{2}\frac{P_{\mathrm{H}}}{\rho_0}\left(\frac{\mu}{1 + \mu}\right) \tag{6}$$

$$\Gamma\rho = \Gamma_0\rho_0 = \mathrm{Const} \tag{7}$$

where ρ denotes the density of the material, Γ denotes the Gruneisen constant, C_0 denotes the sound velocity of the material, S denotes the material constant, and e denotes the inner energy.

The explosive welding model adopts a two-dimensional planar structure, as illustrated in Fig.2, and the line detonation point was positioned at the model's upper left corner to emulate the detonation process triggered by electronic detonator. To facilitate further data acquisition of the explosive welding process, an equidistant array of five measurement points was established between the TC4 and Al 6016 interfaces. The numerical model was constructed based on experimental parameters. The explosive material was discretized by the Eulerian algorithm, while the upper half of the TC4 titanium alloy plate in contact with the explosive was discretized using the ALE algorithm to ensure algorithmic

Table 1 Explosive parameters of JWL equation of state[18]

ρ/g·cm^{-3}	D/m·s^{-1}	P_{CJ}/GPa	γ	A/GPa	B/GPa	R_1	R_2	ω
0.8	2100	1.26	1.8	12.46	0.922	4.41	1.117	0.22

Table 2 Steinberg-Guinan constitutive model parameters

Material	ρ/g·cm^{-3}	G_0/GPa	Y_0/GPa	Y_{max}/GPa	β	n	G'_P	G'_T/GPa·K^{-1}	y'_P
TC4	4.419	41.9	1.33	2.12	12	0.1	0.481 9	−0.026 98	0.015 3
Al 6063	2.703	27.6	0.29	0.68	125	0.1	1.8	−0.017	0.018 908
Al 7075	2.804	26.7	0.42	0.81	965	0.1	1.741	−0.016 45	0.027 38

Table 3 Parameters of the Shock equation of state

Material	Γ	C_0/m·s^{-1}	S_1	S_2	Specific heat/J·kg^{-1}·K^{-1}
TC4	1.23	5130	1.028	0	525
Al 6063	1.97	5240	1.4	0	885
Al 7075	2.2	5200	1.36	0	848

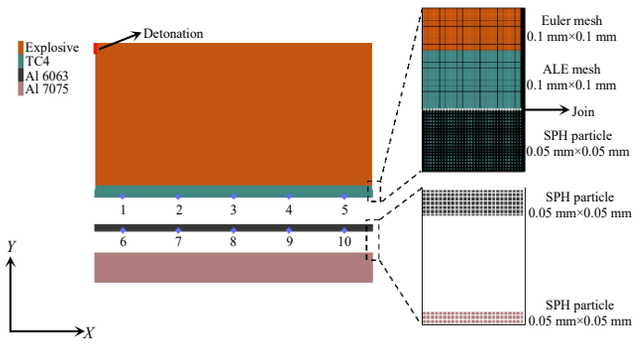

Fig.2 FEM-SPH numerical simulation model

coupling. The lower half of the TC4 titanium alloy plate was modeled with the SPH algorithm, and the Join function was utilized to integrate the FEM mesh with SPH particles, maintaining the model's integrity and preventing the misinterpretation of the two mesh types as distinct entities. Both Al 6063 and Al 7075 were modeled using the SPH algorithm. Regarding mesh division, the explosive material was gridded at 0.1 mm with 0.1 mm intervals, matching the ALE algorithm's grid size of TC4. The SPH algorithm employed a particle size of 0.05 mm for the TC4, Al 6063, and Al 7075. For a model length of 50 mm, the Eulerian grid comprised 125 000 cells, the ALE grid contained 50 000 cells, and the SPH algorithm incorporated 143 143 particles.

2.2 MD simulation method

The simulation process commenced with the creation of single-crystal models using Atomsk, followed by the application of LAMMPS for the computational phase of the numerical analysis. The TC4 alloy was synthesized by integrating 6% aluminum and 4% vanadium into a titanium matrix, forming the desired alloy system. Given that TC4 was primarily composed of α phase at ambient temperatures, a hexagonal close-packed (hcp) lattice was employed for model construction, characterized by lattice parameters of a=0.290 nm and c=0.461 nm[20]. The Al 6063 was modeled using a face-centered cubic (fcc) lattice with a lattice parameter of 0.405 nm[21]. The TC4 titanium alloy exhibits specific crystallographic orientations with respect to the Cartesian coordinate system: $[2\bar{1}\bar{1}0]$ along X-axis, $[\bar{1}2\bar{1}0]$ along Y-axis, and [0001] along Z-axis. In contrast, the Al 6063 alloy demonstrates a simpler alignment, i.e., [100] for X-axis, [010] for Y-axis, and the universally aligned [001] for Z-axis. The model dimensions were 59.755 nm×20.25 nm×9.315 nm, comprising 320 000 atoms for TC4 and 326 600 atoms for Al. The simulation time step was set as 1 fs. The MD computational model is illustrated in Fig.3.

For selecting an appropriate interatomic potential function, this study used a fitting algorithm based on the embedded atom method (EAM). This algorithm encompasses a wide array of metallic elements frequently utilized in various applications[22]. The focus of the current study is a tri-element system, encompassing Ti, Al, and V. Through the application

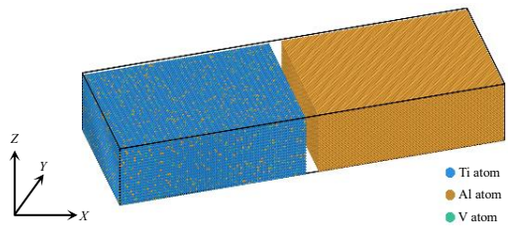

Fig.3 MD simulation model

of the aforementioned fitting algorithm, an EAM potential function tailored for the Ti-Al-V alloy was efficiently constructed. The efficacy of this function has been validated and supported by prior findings.

The MD simulation of explosive welding is delineated into three principal stages: equilibration, loading, and unloading. The equilibration phase is imperative to mitigate any irregularities in the initial modeling structure, ensuring the initial equilibrium and stability of the MD simulation system. This study employed the NPT ensemble at room temperature and zero pressure for a duration of 1000 ps to achieve system stabilization. In the loading phase, the collision velocity between the plates, derived from the ANSYS/AUTODYN 2D simulation, serves as the initial parameter for simulating the atomic-scale bonding process in explosive welding. The NVE ensemble is used during this phase, given that the collision at the bonding interface is instantaneous and can be approximated as an adiabatic process. Upon cessation of the collision motion, the system is further evolved under the NVE ensemble for 500 ps to allow the post-impact stabilization of temperature and pressure. Subsequently, to simulate the unloading phase of the welding process, the MD simulation was executed under the NPT ensemble at equilibrium temperature and zero pressure for additional 1000 ps.

3 Results and Discussion

3.1 Interfacial morphology and element distribution

As depicted in Fig. 4, the interfaces of explosively welded TC4/Al 6063 and Al 6063/Al 7075 display a coexistence of flat and undulating regions, indicating their micro-morphological characteristics. For a more detailed examination of the micro-morphology at the bonding interfaces, the undulating zones highlighted in Fig. 4a and 4c are magnified, as illustrated in Fig. 4b and 4d, respectively. Comparative analysis of the magnified undulating regions reveals that Al 6063/Al 7075 interface exhibits larger wavelengths and amplitudes compared with TC4/Al 6063 interface, and this phenomenon can be ascribed to the variance in material properties, such as hardness and tensile strength, between titanium and aluminum alloys[23]. Extant literature suggests that pronounced undulations at the bonding interface may be conducive to enhanced interfacial bonding[24]. However, the emergence of such undulations can also precipitate defects. In the context of dissimilar titanium/aluminum explosive welding, the genesis of cracks in proximity to the undulating

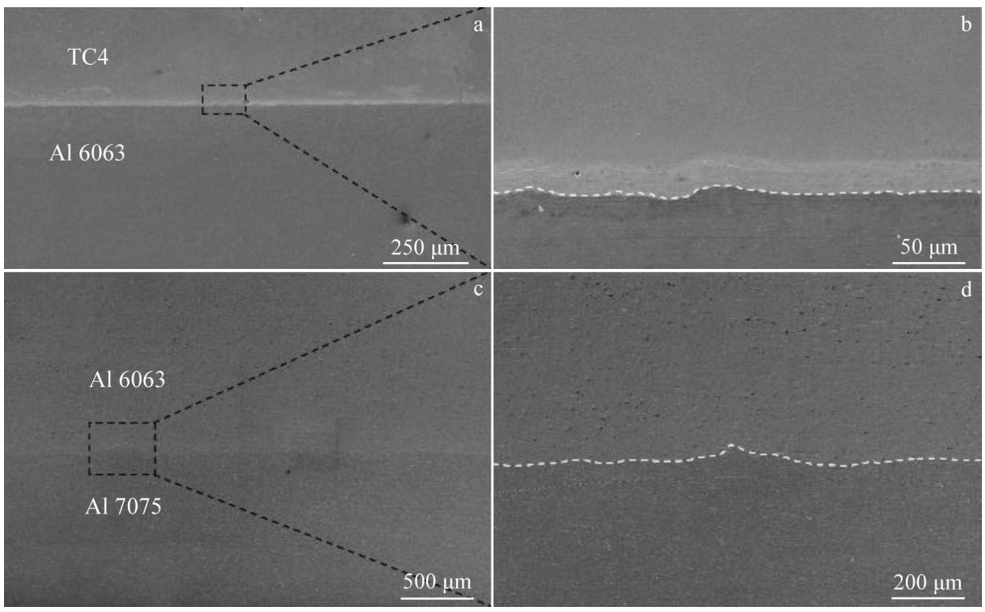

Fig.4 SEM images of TC4/Al 6063/Al 7075 bonding interfaces: (a–b) TC4/Al 6063 interface and (c–d) Al 6063/Al 7075 interface

interface is often related to the formation of brittle intermetallic compounds, which can compromise the integrity of the bond. Furthermore, in the explosive welding of similar metals, the emergence of large undulations is frequently concomitant with the formation of vortex zones, augmenting the likelihood of interfacial melting defects[25]. In localized magnification of two undulating interfaces, no discernible defects are observed in the vicinity of the interfaces, signifying robust bonding quality. Consequently, the presence of large undulations at the bonding interface should not be singularly employed as an indicator of the quality of explosive welding in experimental fabrication processes.

To analyze the elemental distribution characteristics at the TC4/Al 6063 dissimilar metal bonding interface, both surface and line elemental scanning were employed for qualitative and quantitative analysis of the interface elements. As depicted in Fig. 5, a typical undulating TC4/Al 6063 bonding interface is selected, and different elements are distinguished by different colors within the figure. The titanium/aluminum bonding interface does not exhibit a significant melting layer, thus

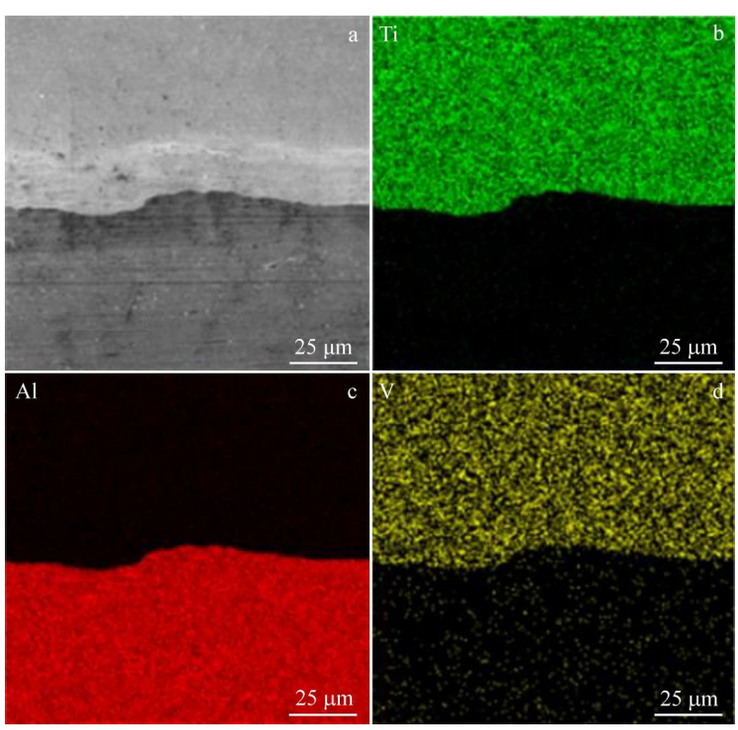

Fig.5 SEM image (a) and EDS element mappings (b–d) of TC4/Al 6063 bonding interface

circumventing the adverse effects of melting layer on the bonding quality. To further confirm the extent of atomic diffusion layer at the joining interface, line elemental scanning is sequentially conducted across various regions of the undulating interface, providing a more comprehensive reflection of the overall elemental situation at the bonding interface, as shown in Fig. 6. The arrows in the figure indicate the element line scanning areas. The results reveal the diffusion and distribution of elements at the bonding interface, and the diffusion thickness of elements is essentially consistent across different regions, measured approximately as 1.6 and 1.7 μm. During the explosive welding process under the impact of explosive shock loading, intense plastic deformation and adiabatic shear occur at the bonding interface, causing a rapid increase in temperature. When the temperature near the interface reaches the melting point and atomic diffusion occurs under the influence of deformation energy, an elemental diffusion layer is ultimately formed[26].

3.2 Grain structure

To further investigate the grain structure and distribution characteristics at the TC4/Al 6063/Al 7075 explosive welding interface driven by explosive detonation, EBSD was used to analyze two bonding interfaces. Fig. 7 and Fig. 8 present the inverse pole figure (IPF) and grain size distribution of TC4/Al 6063 and Al 6063/Al 7075 bonding interfaces, respectively, revealing the size, morphology, and distribution characteristics of grain structures at the interfaces. IPF maps indicate an inhomogeneity in grain size and distribution at both interfaces, with a noticeable refinement of grains near the bonding areas. This suggests that during the explosive welding process, the high-speed collision between the plates generates intense plastic deformation and high temperatures and pressures at the bonding interface area, leading to the generation of dislocations, slip, and shear deformation among grains, which results in grain refinement near the interface and thereby enhances the bonding strength of the welding interface[27].

The grain size statistics for the TC4/Al 6063 interface area are shown in Fig.7b–7c, with an average grain size of 3.24 μm for TC4 and the largest grain size reaching 17 μm. For Al 6063, the average grain size is 4.76 μm, with the largest grain size reaching 40.7 μm. Grains in the TC4 region are significantly smaller than those in the Al 6063 region, due to inherent differences in grain size between the materials. The grain size statistics for the Al 6063/Al 7075 interface area are depicted in Fig.8b, with an average grain size of 4.97 μm and the largest grain size being 41.28 μm. There is a significant difference in grain morphology between Al 6063 and Al 7075 regions, primarily due to different initial grain morphologies obtained from industrial preparation of different series of aluminum alloys[28]. On the Al 7075 side, the Al grains exhibit distinct deformation characteristics; under the action of plastic deformation, grain fracture is accompanied by the formation of twins. The emergence of twin structures increases the slip resistance in the Al 7075 region, hindering the movement of dislocations[29].

Fig.9a and 9c display local average misorientation maps for the TC4/Al 6063 and Al 6063/Al 7075 interfaces, respectively, illustrating the extent and pattern of plastic deformation

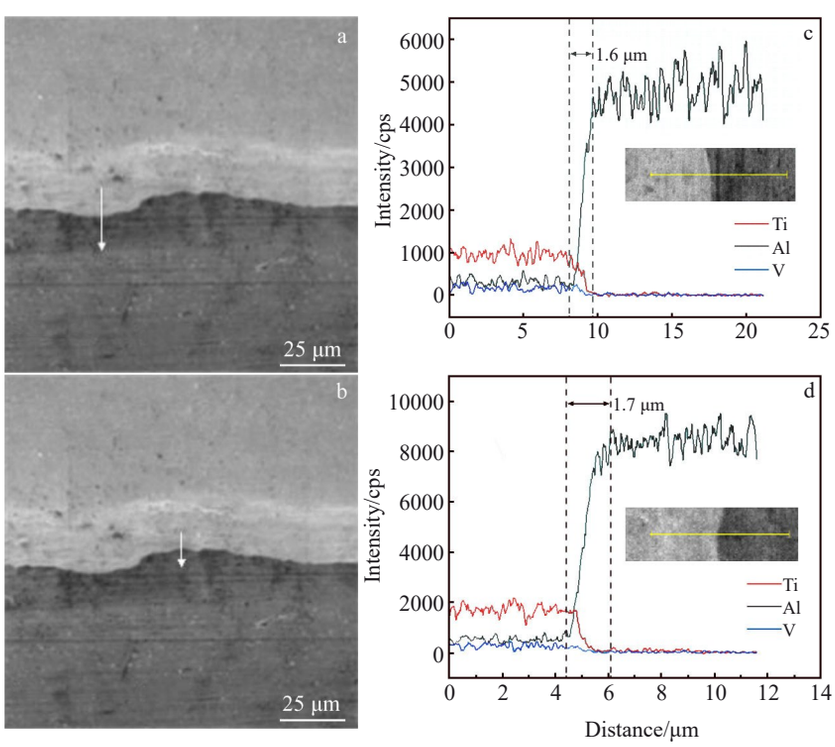

Fig.6 SEM images (a – b) and EDS line scanning results (c – d) of TC4/Al 6063 bonding interface: (a, c) valley region of the interface and (b, d) peak region of the interface

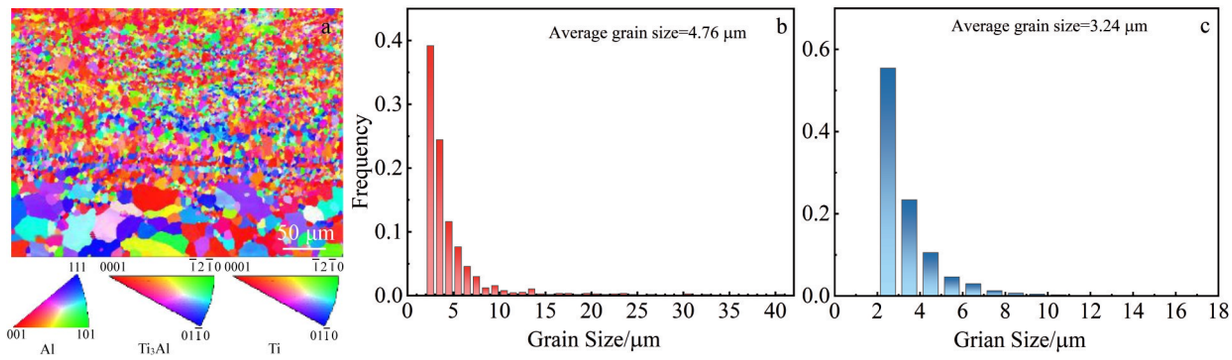

Fig.7 IPF orientation map (a) and grain size distributions (b−c) of TC4/Al 6063 bonding interface: (b) Al 6063 and (c) TC4

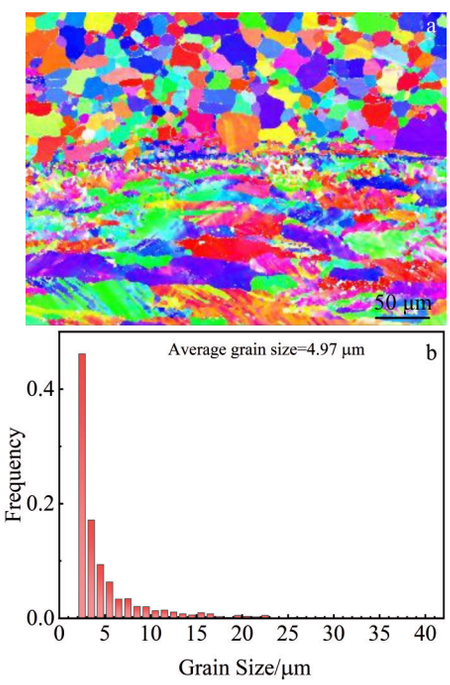

Fig.8 IPF orientation map (a) and grain size distribution (b) of Al 6063/Al 7075 bonding interface

within these regions. As shown in Fig. 9a, TC4 side near the TC4/Al 6063 bonding interface exhibits a significant deviation in orientation compared with Al 6063 side, indicating a higher level of stress within the grains and grain boundaries on the TC4 side during the formation of explosive welding interface. This is attributed to the limited slip systems of the hcp crystal structure of titanium, which are less than those of the fcc crystal structure of aluminum alloys, leading to a weaker stress transmission capability and an increase in internal stress and plastic deformation on the titanium side[30]. At the Al 6063/Al 7075 bonding interface, the orientation deviation is more pronounced on the Al 7075 side, indicating greater internal stress and plastic deformation compared with those on the Al 6063 side.

Fig. 9b and 9d present the recrystallization analysis results for the TC4/Al 6063 and Al 6063/Al 7075 bonding interface regions, respectively. The result brings to light three separate microstructures: deformed structure, recrystallized structure, and substructure. In the TC4/Al 6063 interface region, the proportions of deformed structure, recrystallized structure, and substructure are 58.1%, 9.2%, and 32.7%, respectively. The predominance of the deformed structure corresponds to the distribution of plastic strain observed in Fig. 9a. The recrystallized structure is primarily found within fine Ti grains scattered throughout the region, while the substructure is primarily located within the stretched grains caused by flow deformation. On the Al 6063 side, the percentages of deformed structure, recrystallized structure, and substructure are 5.3%, 56.2%, and 38.5%, respectively. The characteristic large deformation of metallic materials during explosive welding under explosive loading influences the recrystallization microstructure, and greater deformation favors recrystallization and the formation of fine dislocation-free grains[31]. This is consistent with the production of a large number of fine and ultrafine grains on the Al 6063 side (Fig. 7). At the Al 6063/Al 7075 interface, the Al 6063 side is predominantly characterized by recrystallized structures and substructures, due to its relatively lower hardness and strength compared to those of Al 7075, making it more susceptible to large deformation which is conducive to the formation of recrystallized structures. On the Al 7075 side, the deformed structure is the most prevalent, with almost no recrystallized structure present, which aligns with the plastic deformation distribution shown in Fig. 9c. The distribution differences of three structures across the interfaces are mainly attributed to the properties of the metals involved.

3.3 FEM-SPH simulation analysis

To investigate the characteristic variations of the substrate material at the bonding interface of the TC4/Al 6063/Al 7075 composite plate during explosive welding process under the action of explosive detonation loads, a numerical computation method combining FEM and SPH is employed to analyze the morphology, pressure, and temperature distribution at each bonding interface, as shown in Fig. 10. Fig. $10a_1$ illustrates the contact process during the explosive welding of the flyer plate, intermediate layer, and base plate, and the formation of the bonding interface is accompanied by the ejection of metal jet particles. Fig. $10a_2$ is local magnification of the bonding interface in Fig. $10a_1$. It is observed that most areas of the two

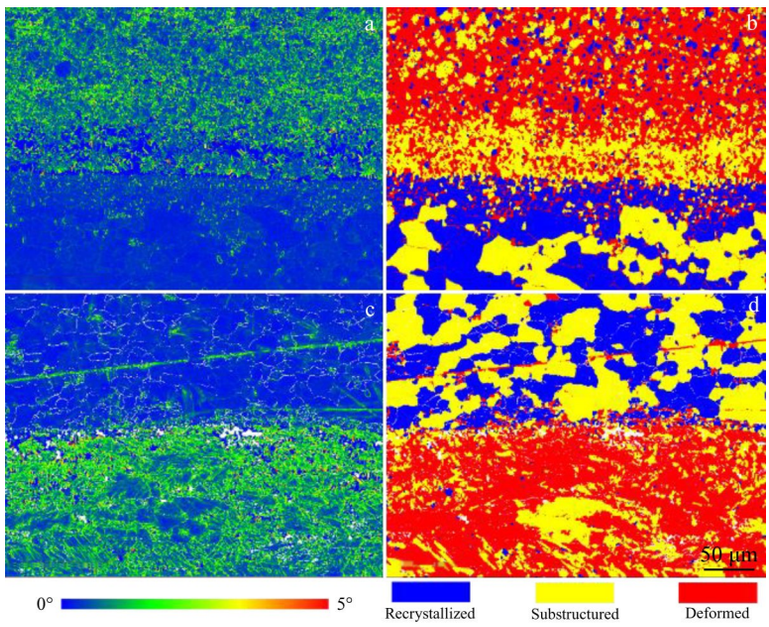

Fig.9 EBSD characterization results (a, c) and recrystallization distribution (b, d) of TC4/Al 6063/Al 7075 bonding interfaces: (a–b) TC4/Al 6063 interface and (c–d) Al 6063/Al 7075 interface

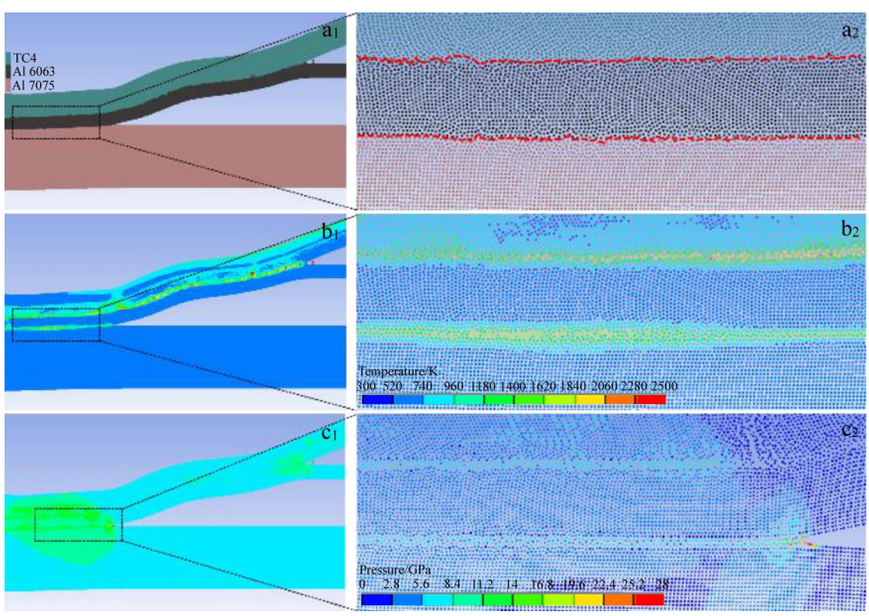

Fig.10 FEM-SPH simulation results of TC4/Al6063/Al7075 bonding interface: (a_1-a_2) morphology features, (b_1-b_2) interfacial temperature distributions, and (c_1–c_2) interfacial pressure distributions

bonding interfaces exhibit a flat keying morphology, and some areas show small wavy morphology. The overall numerical computation results are essentially consistent with the experimental interface characterization results obtained by FESEM. Fig. $10b_1-10b_2$ display the temperature distributions across the interface during the explosive welding process. It can be seen that the temperature at the bonding interface is significantly higher than that in other areas of the plate, primarily due to the high-speed oblique collision at the interface, which converts part of the kinetic energy into thermal energy, forming a high-temperature region. The temperature at the bonding interface is approximately in the range of 1840–2060 K, which exceeds the melting points of the materials used in this experiment, facilitating subsequent diffusion of elements at the interface. Fig. $10c_1-10c_2$ show the pressure distribution at the bonding interface. As the explosive detonation and sliding continue to advance, the high-pressure area at the bonding interface also moves forward. The pressure near the collision area of the interface is significantly higher than that in other regions, with the peak pressure

reaching up to 28 GPa.

For depicting the evolution of effective plastic strain, Fig.11 shows the strain-time profiles at various points along the interface. The measurement points in Fig.11 are shown in the numerical calculation model in Fig. 2. The curves reveal that for a single bonding interface, the effective plastic strain exhibits higher values in the middle and lower values at the sides. This is primarily attributed to the energy released by the explosive detonation which is predominantly concentrated in the central region of the plates, resulting in a greater amount of explosive load energy and enhanced kinetic energy in the central area, which leads to increase in plastic strain between the plates. Furthermore, effective plastic strain curves for different interfaces indicate that the peak value of the effective plastic strain at the measurement point of TC4 side is larger than that at the measurement point of Al 6063 side. This finding is consistent with the EBSD results in Fig.9.

3.4 MD simulation analysis

To analyze the atomic-scale diffusion evolution mechanism at the interface of dissimilar metals during the explosive welding process, MD simulation is initiated with the interfacial collision velocities obtained from FEM-SPH simulation. By extracting the mean square displacement (MSD) data during the loading and unloading phases, a qualitative and quantitative analysis of the diffusion extent and diffusion coefficients of the two phases is conducted, as depicted in Fig. 12. During the loading phase, under the influence of the initial velocity, TC4 and Al collide and compress against each other. The initial MSD curve exhibits oscillations, which later, as the system's kinetic energy is gradually transformed into internal energy, approximates a linear relationship with time. Eventually, the MSD value for the TC4 system stabilizes around 4.3 nm², and for the Al system, it stabilizes around 8.2 nm², as shown in Fig.12a. The

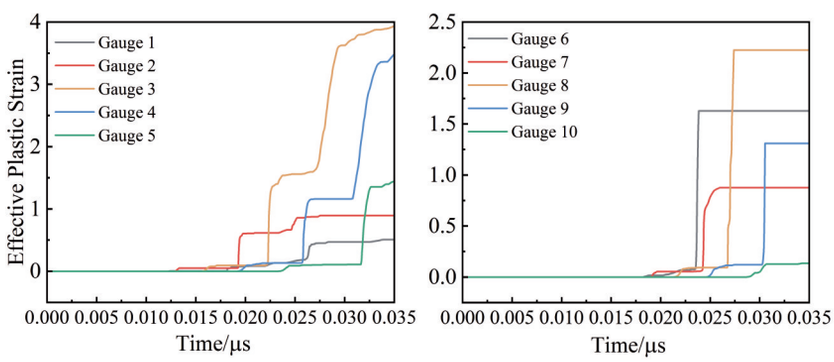

Fig.11 Effective plastic strain-time curves at various points of the bonding interface as marked in Fig.2

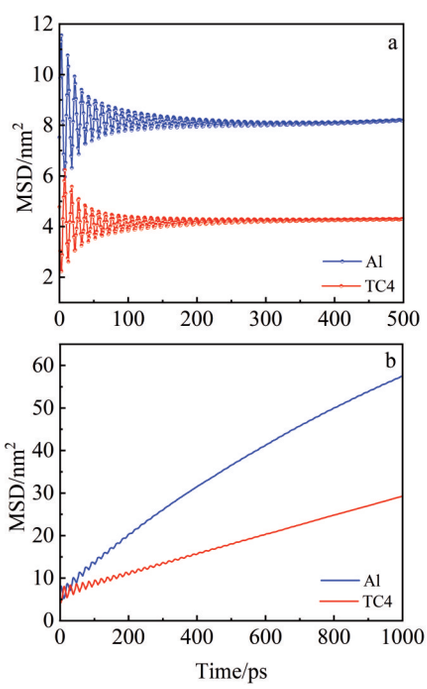

Fig.12 MSD curves along *X*-direction during loading phase (a) and unloading phase (b)

trend of the slope change of MSD curve during the loading phase indicates that only a certain displacement of atoms between the two systems occurs, due to the relative displacement under the external load, without any diffusion phenomenon, and the entire system remains a solid state. Currently, the system temperature is stabilized around 2050 K, exceeding the melting point of the materials in the simulation. The main reason for the lack of diffusion of interfacial atoms during the loading phase is the increase in pressure at the interface due to the collision, which raises the melting point in a high-pressure environment[32]. Post-processing of the MD model after the loading phase with OVITO reveals no diffusion phenomena. In the unloading phase, as the interface forms, the interfacial pressure drops rapidly, and the MSD values for both the TC4 and Al systems increase sharply. When the simulation time reaches 1000 ps, the MSD values for the TC4 and Al systems rise to 29.3 and 57.5 nm², respectively, as illustrated in Fig. 12b. This indicates that during this phase, as the system pressure decreases, TC4 and Al melt at the original system temperature and diffuse towards the opposite system. Analysis of the slopes of the MSD curves of each system reveals that the atomic diffusion rate of the Al system is relatively faster than that of the TC4 system. Observations of the atomic distribution and interfacial

diffusion phenomena at various moments during the unloading phase are conducted using OVITO. Fig. 13 presents the atomic distribution of the system at 100, 400, 700, and 1000 ps during the unloading phase. It is evident that with prolonging the simulation time of the unloading phase, the atomic diffusion phenomena at the interface become increasingly apparent, and the elemental diffusion layers become clearly visible.

3.5 Derivation of interfacial diffusion thickness

Previous studies have indicated that the thickness of the diffusion layer directly influences the performance of the explosive welding interface, hence necessitating further analysis of the interfacial diffusion mechanism and the breadth of the diffusion interface at the atomic scale. Based on conclusions from prior research, it is widely accepted that the elemental diffusion process in explosive welding typically occurs within the range of 10^{-6} – 10^{-5} s. However, current MD simulations are constrained by the limitations of computational performance and cannot achieve calculations for extremely large atomic systems or over exceedingly long time spans. Therefore, by integrating classical interface diffusion theory with results from MD simulations, a formula for calculating the diffusion layer thickness under the experimental conditions of explosive welding has been derived, establishing a range for the diffusion thickness. In the unloading phase, the NPT ensemble conditions prevail, and upon attaining dynamic equilibrium, the diffusion at the weld interface adheres to Fick's second law[33]:

$$\frac{\partial n}{\partial t} = D\nabla^2 n \tag{8}$$

where n is the atomic concentration, t is time, and D is the diffusion coefficient, which is half of the slope of the MSD curve in the unloading stage. The one-dimensional diffusion along the X-axis is the solution of Eq. (8), as expressed as follows:

$$n(x,t) = \frac{N}{2\sqrt{\pi Dt}} \exp\left(-x^2/4Dt\right) \tag{9}$$

From this, the formula for calculating the diffusion thickness can be obtained:

$$y = \sum_{i=\text{TC4, Al}} k\sqrt{D_i t} \tag{10}$$

In the pursuit to elucidate the diffusion mechanism at the atomic scale during the explosive welding process, a meticulous analysis of the interface diffusion phenomena and the consequent diffusion layer thickness is imperative. The diffusion coefficient D_i, denoted by k as a constant dependent on the diffusion conditions, is derived from the MSD curve during the unloading phase of the MD simulation. This coefficient is pivotal as it establishes a linear relationship between the diffusion thickness y and time $\sqrt{t}$. Utilizing the atomic coordinate data extracted from the MD simulated unloading phase at 100 ps with OVITO software, C++ programming was employed to discretize the coordinate area into 500 equal segments along the diffusion direction perpendicular to the interface. By calculating the proportional concentration of atoms within each segment, the atomic concentration distribution along the diffusion axis was constructed. This method allows to ascertain the thickness of the atomic diffusion layer at various specific time, as illustrated in Fig. 14. Subsequently, the diffusion thickness values obtained from the simulation were integrated with the formula deduced from Eq. (10) to perform a data fit, thereby revealing the correlation between the diffusion layer thickness and the diffusion time. This relationship is depicted in Fig. 15. In line with previous studies, the unloading phase of explosive welding is generally estimated to span between 5 and 10 μs[34]. According to the diffusion layer thickness formula derived from Fig. 15, the theoretical calculation of the diffusion layer thickness is anticipated to fall within the range of 1.40–1.98 μm. The line scanning characterization of the welding interface yields an average diffusion layer thickness of 1.65 μm. The consistency between the theoretical values deduced from the MD simulation and diffusion theory with the experimental findings substantiates the authenticity and reliability of our simulation outcomes.

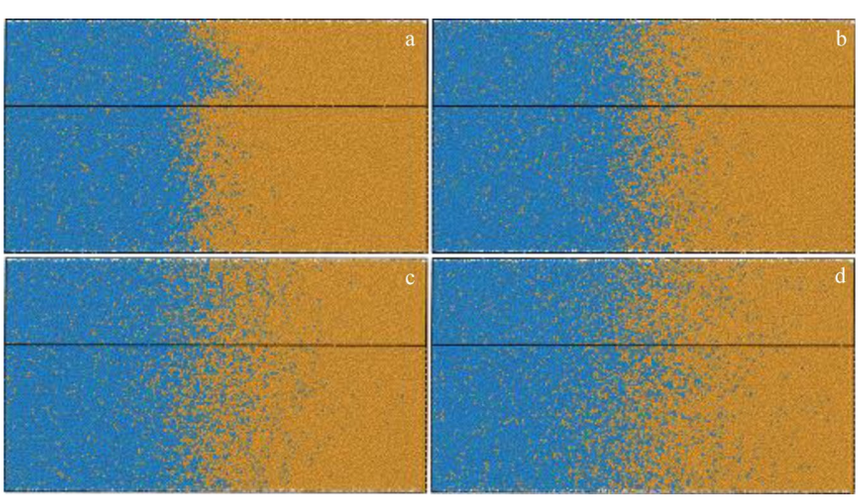

Fig.13 Distributions of atoms in the unloading phase: (a) 100 ps, (b) 400 ps, (c) 700 ps, and (d) 1000 ps

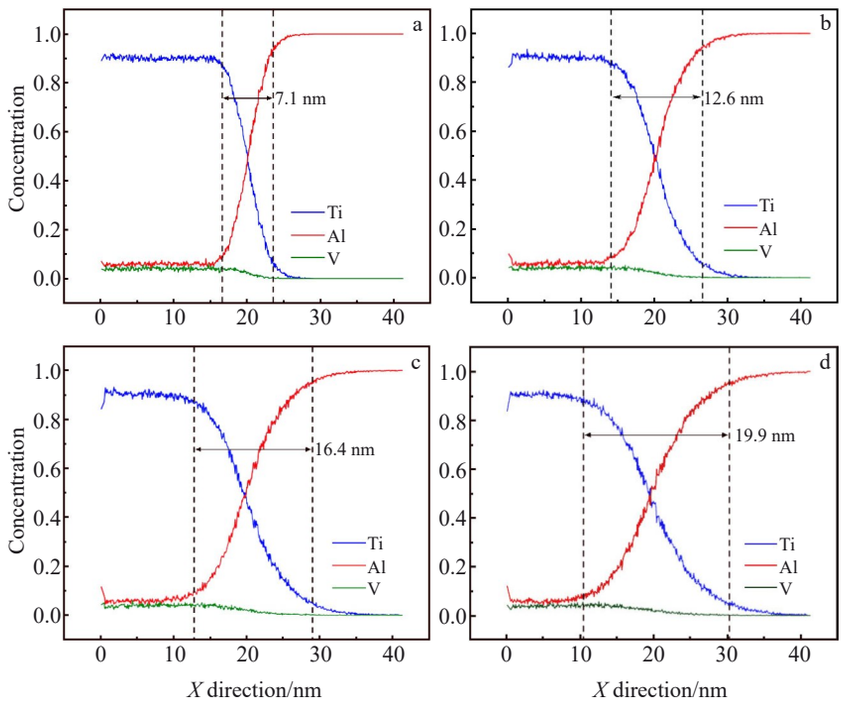

Fig.14 Simulation results of diffusion layer thickness in unloading phase: (a) 100 ps, (b) 400 ps, (c) 700 ps, and (d) 1000 ps

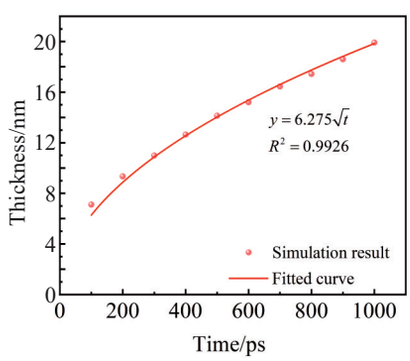

Fig.15 Fitting and derivation of diffusion layer thickness

4 Conclusions

1) The use of explosive welding technology, with the introduction of an intermediate layer, is an effective way to obtain lightweight and high-strength titanium-aluminum alloy composite plates. Both the TC4/Al 6063 and Al 6063/Al 7075 bonding interfaces exhibit good bonding quality without obvious defects or cracks. The interface morphology shows flatness and small undulations, with an average diffusion layer thickness of 1.65 μm at the TC4/Al 6063 bonding interface.

2) Due to the high temperature, high pressure, and intense plastic deformation during the formation of the two bonding interfaces, grain refinement phenomena occur near the interfaces, and obvious twin structures are observed within the Al 7075 region. At the same time, under the action of strong impact loads, the degree of plastic deformation of both TC4 and Al 7075 at two bonding interfaces is greater than that of the intermediate layer Al 6063.

3) The interfacial morphology obtained from the FEM-SPH numerical simulation matches well with the experimental results, verifying the feasibility of the model. By comparing the interface temperatures from the FEM-SPH simulation and the MD simulation results, it is found that the temperature near the bonding interface is higher than that on both sides of the plate, and the interface temperatures obtained from different simulations are similar, confirming the feasibility of the multi-scale simulation method.

4) The MD simulation results show that the diffusion phenomenon of interface elements mainly occurs during the unloading phase of explosive welding, and the diffusion coefficient of Al is greater than that of TC4. By combining classical diffusion theory with the results of the MD simulation, the diffusion thickness of the interface elements is determined to be 1.40–1.98 μm, which is close to the experimental test result of 1.65 μm, verifying the reliability of the simulation results

References

1 Dai G, Liu Y, Chen K *et al. Journal of Manufacturing Processes*[J], 2023, 103: 78

2 Kazancı Z. *Progress in Aerospace Sciences*[J], 2016, 81: 49

3 Liu M, Zhang C, Meng Z *et al. Composites Part B: Engineering*[J], 2022, 230: 109507

4 Yu M, Zhao H, Jiang Z *et al. Journal of Materials Science & Technology*[J], 2019, 35(8): 1543

5 Li Z, Peng W, Chen Y *et al. Journal of Manufacturing Processes*[J], 2022, 83: 290

6 Ma X, Cao R, Dong H *et al. Rare Metal Materials and Engineering*[J], 2024, 53(4): 1002

7 Chen W, He W, Luo N *et al. Materials Science and Engineering A*[J], 2022, 859: 144230

8 Liang H L, Chen Y, Luo N *et al. Journal of Materials Research and Technology*[J], 2022, 18: 4228

9 Zhou J, Luo N, Liang H L *et al. Journal of Manufacturing Processes*[J], 2024, 124: 1180

10 Wang D, Sun Y, Xue Z *et al. Rare Metal Materials and Engineering*[J], 2023, 52(11): 3723

11 Qin L, Wang J, Wu Q *et al. Journal of Alloys and Compounds*[J], 2017, 712: 69

12 Zang C, Liu J, Tan C *et al. Journal of Manufacturing Processes*[J], 2018, 32: 595

13 Li X, Cheng Y, Zhu S *et al. Vacuum*[J], 2024, 225: 113270

14 Li D, Cheng Y, Xu J *et al. Vacuum*[J], 2024, 227: 113432

15 Bataev I A, Tanaka S, Zhou Q *et al. Materials & Design*[J], 2019, 169: 107649

16 Sun Z, Shi C, Shi H *et al. Materials & Design*[J], 2020, 195: 109027

17 Nguyen V, Thu Nhu V T, Vo X. *Computers in Biology and Medicine*[J], 2024, 174: 108471

18 Xia Z, Wang H, Shi C *et al. Crystals*[J], 2023, 13(7): 1079

19 Liang H L, Luo N, Shen T *et al. Journal of Materials Research and Technology*[J], 2020, 9(2): 1539

20 Ma K, Sun H, Qi Y *et al. Physics Letters A*[J], 2023, 481: 129000

21 Zhang T, Wang W, Zhou J *et al. Acta Metallurgica Sinica (English Letters)* [J], 2017, 30(10): 983

22 Zhao S, Xiong Y, Ma S *et al. Acta Materialia*[J], 2021, 219: 117233

23 Lipińska M, Ura-Bińczyk E, Mróz S *et al. Journal of Manufacturing Processes*[J], 2023, 105: 84

24 Zhu L, Zhou Q, Song C *et al. Journal of Materials Research and Technology*[J], 2024, 28: 668

25 Yang M, Cao C, Wang J. *Materials & Design*[J], 2023, 235: 112372

26 Sun Y, Liu X, Wang W *et al. Journal of Materials Science & Technology*[J], 2023, 144: 150

27 Xu J, Ma H, Yang M *et al. Materials & Design*[J], 2022, 218: 110716

28 Wang T, Sinha S, Komarasamy M *et al. Journal of Materials Processing Technology*[J], 2020, 278: 116460

29 Liang H L, Chen Y, Luo N *et al. Journal of Materials Research and Technology*[J], 2023, 24: 2562

30 Wang X, Cai Y, Shi C. *Journal of Applied Physics*[J], 2024, 135(22): 225108

31 Huang J, Liang G, Luo N *et al. Journal of Materials Research and Technology*[J], 2023, 27: 2508

32 Ma Y, Zhang S, Wang T *et al. Materials Today Communications*[J], 2022, 31: 103552

33 Chen S, Wu Z, Liu K. *Chinese Physics B*[J], 2014, 23(6): 66802

34 Yan H H, Qu Y D, Li X J. *Combustion, Explosion, and Shock Waves*[J], 2008, 44(4): 491

TC4/Al 6063/Al 7075爆炸焊接复合板的微观结构分析：多尺度模拟与实验研究

周嘉楠[1,2]，罗　宁[1,2]，梁汉良[2]，陈金华[2]，刘治兵[2]，周晓红[2]

(1. 中国矿业大学 深地工程智能建造与健康运维全国重点实验室，江苏 徐州 221116)

(2. 中煤科工集团淮北爆破技术研究院有限公司，安徽 淮北 235000)

摘　要：轻质高强钛/铝合金由于材料属性差距悬殊导致复合困难。提出引入Al 6063中间层，通过爆炸焊接成功制备TC4/Al 6063/Al 7075三层复合板。通过场发射扫描电子显微镜和电子背散射衍射揭示了各结合界面微观特性。应用有限元方法-光滑粒子流体动力学（FEM-SPH）方法与分子动力学（MD）方法相结合针对爆炸焊接结合界面多尺度下成形及演化特征进行分析。结果表明，TC4/Al 6063和Al 6063/Al 7075结合界面形貌平坦且存在小波纹，无明显缺陷和裂纹。两个结合界面附近均观察到晶粒细化现象，且TC4与Al 7075塑性变形程度均强于中间层Al 6063。FEM-SPH模拟得到的界面形貌特征与实验结果相近。MD模拟表明，界面元素扩散主要发生在卸载阶段，界面元素扩散厚度模拟结果与测试结果相符。采用引入中间层爆炸焊接工艺可以有效地制备高质量钛/铝合金复合板，并为爆炸焊接结合界面提供了一种多尺度模拟思路。

关键词：TC4/Al 6063/Al 7075复合板；爆炸焊接；微观结构分析；多尺度模拟

作者简介：周嘉楠，男，2000年生，博士生，中国矿业大学深地工程智能建造与健康运维全国重点实验室，江苏 徐州 221116，电话：0516-83590666，E-mail：jnzhou@cumt.edu.cn